# Lattice dynamics and temperature-dependent Raman and infrared studies of multiferroic $Mn_{0.85}Co_{0.15}WO_4$ and $Mn_{0.97}Fe_{0.03}WO_4$ crystals

M. Maczka,[1] M. Ptak,[1] K. Hermanowicz,[1] A. Majchrowski,[2] A. Pikul,[1] and J. Hanuza[1,3]

[1]*Institute of Low Temperature and Structure Research, Polish Academy of Sciences, P.O.Box 1410, 50-950 Wroclaw 2, Poland*

[2]*Institute of Applied Physics, Military University of Technology, 2 Kaliskiego Str., 00-908 Warszawa, Poland*

[3]*Department of Bioorganic Chemistry, University of Economics, 53-345 Wroclaw, Poland*

(Received 25 February 2011; revised manuscript received 12 March 2011; published 25 May 2011)

Lattice dynamics calculations, and temperature-dependent Raman scattering and IR studies of $Mn_{0.97}Fe_{0.03}WO_4$ and $Mn_{0.85}Co_{0.15}WO_4$ crystals are presented. These studies were complemented by magnetization and specific heat measurements for $Mn_{0.85}Co_{0.15}WO_4$. Symmetries of all IR-active modes were established and assignment of the modes to respective motions of atoms was proposed. Low-temperature phonon anomalies were identified, which were attributed to the onset of magnetic order. Our results also revealed an unusual downturn of phonon shifts below 100–200 K for some phonons, which are likely related to some subtle structural changes due to the anisotropic character of thermal expansion. The obtained results also revealed differences in the temperature dependence of Raman- and IR-active phonons for $Mn_{0.97}Fe_{0.03}WO_4$ and $Mn_{0.85}Co_{0.15}WO_4$, which reflect differences in magnetic and ferroelectric properties of the both crystals.

DOI: 10.1103/PhysRevB.83.174439 PACS number(s): 78.30.Hv, 63.20.−e, 75.50.Ee, 77.84.Bw

## I. INTRODUCTION

Multiferroic materials have recently attracted much attention due to their unique magnetic and electric properties, i.e., coexistence of spontaneous polarization and magnetization in the same phase. This group of compounds contains mainly transition-metal oxides, for instance, $Ni_3V_2O_8$,[1] $CuFeO_2$,[2] and $DyMnO_3$.[3] Simple tungstate $MnWO_4$ is one of well-known magnetoelectric multiferroics in which ferroelectricity is induced through the noncollinear spin structure at low temperatures.[4–6] $MnWO_4$ has also been found a prospective material for application as a humidity sensor and efficient catalyst for organic dye photodegradation in sunlight.[7–9]

It has been reported that three antiferromagnetic ordered phases occur in the $MnWO_4$ system: a collinear commensurate structure AF1 ($T \leqslant T_{N1} \approx 6.5-8$ K), a tilted-eliptical structure AF2 ($T_{N1} \leqslant T \leqslant T_{N2} \approx 12.5$ K), and a sinusoidal incommensurate magnetic structure AF3 ($T_{N2} \leqslant T \leqslant T_{N3} \approx 13.5$ K).[6] The intermediate AF2 phase is also ferroelectric, in which spontaneous polarization can be controlled by an internal magnetic field.[5,6] Other wolframite-type crystals $AWO_4$ (A = Fe, Co, Ni) exhibit only one magnetic phase transition at 68, 67, and 55 K for Fe, Co, and Ni tungstate, respectively.[10–12] Doping of $MnWO_4$ with $Fe^{2+}$ causes suppressing of the ferroelectric AF2 phase at H = 0 T, which is recovered by applying the internal magnetic field above 4 T.[13] A different situation is observed in crystals doped with $Co^{2+}$ ions. It has been reported that $Co^{2+}$ doping at x = 0.05 stabilizes the AF2 phase down to the lowest temperature and, as the Co concentration increases further, the spiral-basal plane tilts off the *b* axis and coexists with a simple collinear antiferromagnetic phase AF4.[14,15] However, recent studies of $Mn_{0.85}Co_{0.15}WO_4$ do not confirm tilting of the basal plane since they show that the ferroelectric polarization is observed along only the *b* axis.[16] Furthermore, these studies detected up to four different magnetic structures, and the ferroelectric polarization was associated with both AF2 and AF5 phases.[16]

Raman and IR spectroscopes are known to be powerful probes for understanding details of structural changes and spin-phonon and crystal-field-phonon interactions in magnetic and ferroelectric materials.[17–19] They have also been successfully employed in studies of some multiferroelectrics, for instance $RMn_2O_5$ (R = Bi, Dy, Eu) and $BiFeO_3$.[20,21] Very recently, two papers reporting temperature-dependent Raman spectra of $MnWO_4$ were published. The studies of Iliev *et al.* did not reveal any detectable phonon anomalies near the three successive magnetic and ferroelectric phase transitions.[22] On the other hand, Hoang *et al.* observed weak anomalies for the 884.4-, 697.7-, and 673.3-$cm^{-1}$ phonons near 180 K and for the 272.6-, and 293.6-$cm^{-1}$ phonons near 50 K.[23] The anomaly near 180 K was attributed to a microscopic structural change.[23] IR spectra of $MnWO_4$ have been reported to our knowledge, in only one paper.[24] Wave numbers of IR-active transverse optical (TO) phonons were reported for three different polarization directions on the basis of reflectance spectra and Kramers–Kronig analysis.[24] However, no information on wave numbers of longitudinal optical (LO) phonons was extracted from the reflectance spectra. Furthermore, the absorption spectrum of the polycrystalline sample was not measured and no assignment of the IR-active phonons was proposed. Reference 24 also reported temperature-dependent IR reflectance studies of $MnWO_4$. However, temperature dependence was presented for only four TO phonons and five different temperatures.[24] This study showed no anomalies across the transition temperatures.

This paper reports detailed Raman and IR temperature-dependent studies of $Mn_{0.97}Fe_{0.03}WO_4$ and $Mn_{0.85}Co_{0.15}WO_4$ single crystals in order to obtain information on the influence of $Fe^{2+}$ and $Co^{2+}$ doping on phonon and structural properties of $MnWO_4$. We also present low-temperature magnetization and specific heat for $Mn_{0.85}Co_{0.15}WO_4$. The concentration of $Co^{2+}$ impurity was chosen on the basis of temperature-molar-fraction phase transition diagrams to obtain material within the broad range of occurrence of the ferroelectric phase possessing a large ferroelectric polarization.[14] We will present a detailed assignment of the observed Raman- and IR-active phonons to the respective motions of atoms based on IR- and Raman-polarized studies as well as lattice dynamic (LD) calculations. We will also show that some IR and Raman phonons show an

 

anomalous temperature dependence on wave numbers at low temperatures. The origin of these anomalies will be discussed.

## II. EXPERIMENTAL

MnWO4 crystals melt congruently at 1574 K, so they can be grown from stoichiometric melts by means of the top-seeded technique.[25] However, at this elevated temperature the melt is slightly volatile and the control of growth conditions is difficult. Owing to this we used a high-temperature solution growth method to obtain $Mn_{0.85}Co_{0.15}WO_4$ single crystals. Wanklyn used $Na_2WO_4$ as the solvent in the flux growth of this material.[26] In our experiments $Na_2W_2O_7$ was chosen as the solvent, by analogy to crystallization of double tungstates, like $KHo(WO_4)_2$, from $K_2W_2O_7$ solvent.[27] Crystallization was carried out from a Pt crucible placed in a two-zone resistance furnace under conditions of low-temperature gradients. In the first experiments $Mn_{0.85}Co_{0.15}WO_4$ crystals were obtained by means of spontaneous crystallization from 30 mol% solution of $Mn_{0.85}Co_{0.15}WO_4$ in $Na_2W_2O_7$. The as-grown crystals were extracted from the solidified melt by use of hot water and used as seeds. The top-seeded solution growth was carried out from 15 mol% solutions. No pulling was used, the seeds were rotated at a rate of 30 rpm, and the crystallization was stopped by disconnecting the growing crystals from the melt. The typical rate of cooling was equal to 0.2 K/h, the seed was immersed into the melt at about 1240 K, and the process lasted at least 1 week. The as-grown crystals were cooled down to the room temperature at a rate growing from initial 5 K/h to 10 K/h. Dark graphite plates with dimensions up to 5(a) × 12(b) × 2(c) $mm^3$ were obtained and identified on the basis of x-ray diffraction (XRD) pattern.

Single crystals of $Mn_{0.97}Fe_{0.03}WO_4$ were grown from the stoichiometric melt of MnO and $WO_3$ in $Na_2WO_4$ as a solvent at a molar ratio of 1:1. The mixture of powdered substrates in the platinum crucible was heated to 1250 ° C, held for 20 h, and cooled down at a rate of 1.8°C/h to 1000 ° C and finally cooled to room temperature with a rate 4.8 ° C/h. Dark graphite plates with dimensions up to $1(a) \times 4(b) \times 7(c)$ $mm^3$ were obtained.

Both $Mn_{0.97}Fe_{0.03}WO_4$ and $Mn_{0.85}Co_{0.15}WO_4$ crystals for the spectroscopic studies were oriented using the XRD method.

The polarized Raman spectra were measured using a Bruker FT 100/S spectrometer with YAG:Nd laser excitation (1064 nm). The resolution was 2 $cm^{-1}$. The orientation of the crystallographic axes was done using an x-ray method. The temperature-dependent spectra were measured using a helium-flow Oxford cryostat.

Polycrystalline IR spectra were measured as KBr pellets in the 1500–400 $cm^{-1}$ region and in Nujol suspension for the 500–50 $cm^{-1}$ region. Polarized spectra of the single crystals were measured at near-normal incidence using a specular reflectance accessory. The spectral resolution was 2 $cm^{-1}$.

Magnetization and specific heat of single-crystalline $Mn_{0.85}Co_{0.15}WO_4$, were investigated employing commercial Quantum Design magnetic property measurement system and physical property measurement system platforms, respectively. The magnetization was measured for an unoriented single crystal. For calorimetric experiments, one single crystal of the compound was used together with a small amount of vacuum grease Apiezon N as a sample mounting medium. While the magnetization of the sample holder used in the magnetic properties measurement was found to be negligible in comparison with the total signal measured, the heat capacity of the microcalorimeter with the grease was carefully subtracted from the total specific heat measured.

## III. RESULTS AND DISCUSSION

### A. Room-temperature crystal structure of $MnWO_4$

To understand the phonon properties of $MnWO_4$ and their temperature dependence, it is important to provide a brief discussion of the crystal structure at ambient pressure and room temperature. $MnWO_4$ crystallizes in a monoclinic structure (space group symmetry $P2/c = C_{2h}^4$) and its lattice parameters are $a = 4.830(1), b = 5.7603(9), c = 4.994(1)$ Å, $\beta = 91.14(2)^\circ$ and Z = 2.[28] The crystal structure of $MnWO_4$ (see Fig. 1) is built up of $Mn^{2+}$ cations and deformed $WO_6$ octahedra which form the edge-sharing zigzag-like chains along the crystallographic *c* axis. The $WO_6$ units are connected by a double oxygen bridge with shorter and longer W–O1 distances of 1.9038 and 2.1264 Å, respectively.[28] The second type of tungsten-oxygen bonds, i.e., W–O2 bonds which do not participate in formation of oxygen bridges, are shorter (1.7978 Å). The W and Mn atoms occupy the 2*e* and 2*f* positions, respectively, of $C_2$ symmetry, and all oxygen atoms are located at general positions.[28]

### B. Lattice dynamic calculations and assignment of modes

A standard group-theoretical analysis for the P2/c room-temperature phase of $MnWO_4$ containing 12 atoms in the unit cell leads to $8A_g + 7A_u + 10B_g + 8B_u$ optical modes and $A_u + 2B_u$ acoustic modes. Lattice translational modes of the Mn and W atoms contribute to the $2A_g + A_u + 4B_g + 2B_u$ optical modes, and symmetric (antisymmetric) stretching and bending vibrations of the double WOOW oxygen bridge contribute to the $3A_g + 3B_g$ ($3A_u + 3B_u$) modes. Vibrations of the $WO_2$ groups (with short W–O2 bonds) give rise to $A_g + A_u$

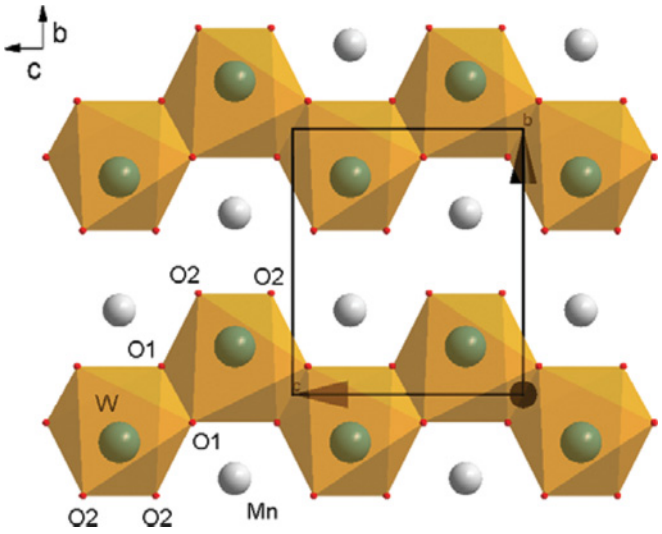


FIG. 1. (Color online) View of the $MnWO_4$ crystal structure along the *a* axis.

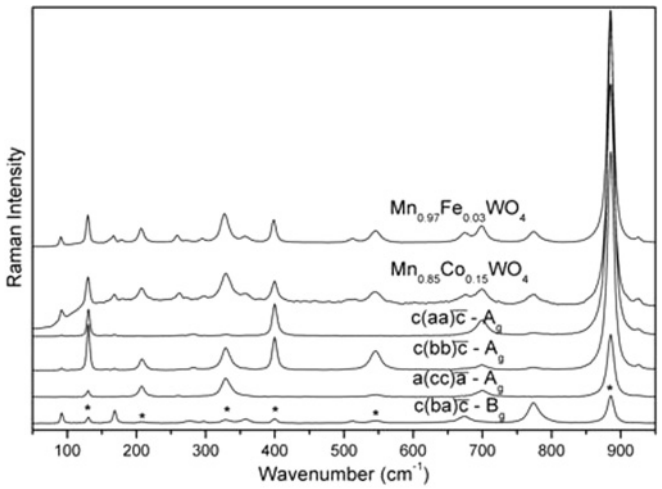


FIG. 2. Raman spectra of polycrystalline tungstates and polarized Raman spectra of a $Mn_{0.85}Co_{0.15}WO_4$ single crystal. Asterisks denote bands, which correspond to $A_g$ modes and appear in the c(ba)c spectrum due to polarization leakage.

($B_g$+ $B_u$) symmetric (antisymmetric) stretching ($\nu_s$ and $\nu_{as}$), $A_g$+ $A_u$ scissoring ($\delta_{sc}$), $B_g$+ $B_u$ rocking ($\rho$), $A_g$+ $A_u$ twisting ($\tau$), and $B_g$+ $B_u$ wagging modes ($\omega$). Selection rules show that all $g$ modes ($8A_g + 10B_g$) are Raman active and all $u$ modes ($7A_u$+$8B_u$) are IR active.

The recorded Raman and IR spectra are presented in Figs. 2 and 3, respectively. The IR reflection spectra, presented in Fig. 3, were fitted by using a four-parameter model to give information about TO and LO wave numbers.[29] According to this model, the complex dielectric constant is expressed in terms of the IR-active modes as follows:

$$\varepsilon(\omega) = \varepsilon_\infty \prod_j \frac{\omega_{jLO}^2 - \omega^2 + i\omega\gamma_{jLO}}{\omega_{jTO}^2 - \omega^2 + i\omega\gamma_{jTO}}, \quad (1)$$

where $\omega_{jTO}$ and $\omega_{jLO}$ correspond to the resonance frequencies of the *jth* transversal and longitudinal modes, respectively, and $\gamma_{jTO}$ and $\gamma_{jLO}$ are the corresponding damping factors. $\varepsilon_\infty$ is the high-frequency dielectric constant. For normal incidence, the IR reflectivity $R$ and the dielectric function are related by

$$R = \left|\frac{\sqrt{\varepsilon} - 1}{\sqrt{\varepsilon} + 1}\right|^2. \quad (2)$$

The results of fitting of the experimental data to the four-parameter model are shown in Figs. 3(c) and 3(d), and Table I, which also lists Raman wave numbers. The absorption coefficient presented in Fig. 3(c) is related to the imaginary part of the dielectric function by

$$\alpha = \varepsilon''(\omega)\omega/nc, \quad (3)$$

where $n$ denotes the refractive index and $c$ is the speed of light. One can also calculate the static dielectric constant from the phonon contributions as

$$\varepsilon_0 = \varepsilon_\infty + \sum \Delta\varepsilon_j. \quad (4)$$

Our values of $\varepsilon_0$ at 300 K are 21.4, 18.9, and 30.5 for the light polarized along the *a, b*, and *c* axes, respectively. A former low temperature study of $MnWO_4$ reported an ~16.5 value for

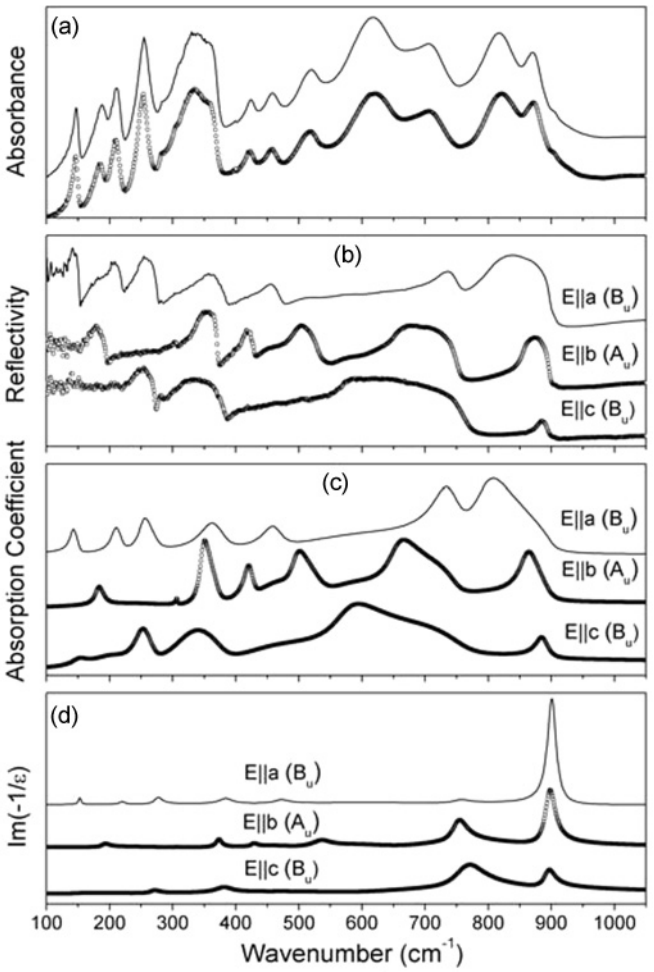


FIG. 3. IR absorption spectra of (a) polycrystalline and (b) reflectivity data of $Mn_{0.85}Co_{0.15}WO_4$ (solid lines) and $Mn_{0.97}Fe_{0.03}WO_4$ (circles). Panels (c) and (d) show the calculated wave-number dependence of the absorption coefficient $\alpha$ ($\alpha = 2\omega$k/c, where k is the extinction coefficient and c is the speed of light) and the imaginary part of the inverse dielectric function, respectively.

$\varepsilon_b$ at 20 K, whereas the study of $Mn_{0.85}Co_{0.15}WO_4$ reported 10.66 and 9.19 values at 25 K for $\varepsilon_a$ and $\varepsilon_b$, respectively.[6,16]

The calculations of wave numbers and displacement vectors were performed on the basis of a partially ionic model described previously.[30] The ionic shell model treats the material as a collection of core-shell systems (symbolizing nuclei and electron shell) interacting with each other through electrostatic and short-range classic potentials. The following interatomic potential is taken into account:

$$U_{ij}(r_{ij}) = \frac{z_i z_j e^2}{r_{ij}} + b_{ij}\exp\left[\frac{-r_{ij}}{\rho_{ij}}\right] - \frac{c_{ij}}{r_{ij}^6}. \quad (5)$$

The first term is related to the Coulomb forces for modeling the long-range interactions. The second term is related to the Born–Mayer-type repulsive interaction for accounting for the short-range forces. A van der Waals attractive interaction (third term) models the dipole-dipole interaction. $z_i$ and $z_j$ are the effective charges of the $i$ and $j$ ions, respectively, separated by the distance $r_{ij}$. The parameters $\rho_{ij}$ and $b_{ij}$ correspond to the ionic radii and ionic stiffness, respectively.

TABLE I. Room-temperature experimental and calculated (calc) Raman and IR wave-numbers together for polycrystalline (poly) and single crystals with the proposed assignment. For the IR-active mode, the LO wave-numbers are given in parentheses. $B_u$ modes of $MnWO_4$:Co and $MnWO_4$:Fe have been established from the reflection spectra measured with light polarized along the *a* and *c* crystallographic axis, respectively. Sym denotes symmetry of the observed IR mode and sh, vw, w, m, s, and vs denote shoulder, very weak, weak, medium, strong, and very strong, respectively.

| Infrared | | | | | | Raman | | | | |
|---|---|---|---|---|---|---|---|---|---|---|
| | $MnWO_4$:Co | | $MnWO_4$:Fe | | | | Experimental | | | |
| Sym | Crystal | Poly | Crystal | Poly | Calc | Sym | Fe | Co | Calc | Assignment |
| ? | | 905sh | | 905sh | | | 924 vw | 924 vw | | impurity |
| $B_u$ | | | 885 (895) | | | | | | | ? |
| $A_u$ | 855 (897) | 871 m | 861 (897) | 872 m | 837 | $A_g$ | 884 vs | 885 vs | 870 | $\nu_s(WO_2)$ |
| $B_u$ | 795 (901) | 817 s | | 821 s | 777 | $B_g$ | 773 w | 772 w | 812 | $\nu_{as}(WO_2)$ |
| $B_u$ | 733 (756) | | 739 (766) | | | | | | | ? |
| $A_u$ | 653 (757) | 705 m | 656 (753) | 706 m | 671 | | | | | $\nu_{as}$(W-O-W) |
| | | | | | | $A_g$ | 698 w | 700 w | 699 | $\nu_s$(W-O-W) |
| | | | | | | $B_g$ | 673 w | 674 w | 716 | $\nu_s$(W-O-W) |
| $B_u$ | | 617 s | 577 (739) | 620 s | 576 | | | | | $\nu_{as}$(W-O-W) |
| | | | | | | $A_g$ | 545 w | 545 w | 555 | $\delta_s$(W-O-W) |
| $A_u$ | 499 (536) | 517 m | 495 (536) | 515 m | 547 | | | | | $\nu_{as}$(W-O-W) + $\delta_{sc}(WO_2)$ |
| | | | | | | $B_g$ | 511 vw | 511 vw | 480 | $\nu_s$(W-O-W) |
| $B_u$ | 458 (472) | 457 m | | 456 m | 467 | | | | | $\delta_{as}$(W-O-W) |
| $A_u$ | 418 (430) | 424 w | 420 (428) | 422 w | 455 | | | | | $\delta_{as}$(W-O-W) + $\tau(WO_2)$ |
| | | | | | | $A_g$ | 398 m | 400 m | 468 | $\nu_s$(W-O-W) |
| $A_u$ | 344 (372) | 360 s | 348 (373) | 362 s | 410 | | | | | $\delta_{sc}(WO_2)$ + $\tau(WO_2)$ |
| | | | | | | $B_g$ | 357 vw | 356 vw | 443 | $\delta_s$(W-O-W) + $\rho(WO_2)$ |
| $B_u$ | 359 (384) | 328 s | 324 (382) | 330 s | 323 | | | | | $\delta_{as}$(W-O-W) + $\rho(WO_2)$ |
| | | | | | | $A_g$ | 326 m | 328 m | 376 | $\delta_{sc}(WO_2)$ + $\delta_s$(W-O-W) |
| $A_u$ | 311 (312) | 311 sh | 307 (308) | 307 sh | 246 | | | | | $\tau(WO_2)$ + $\delta_{sc}(WO_2)$ |
| | | | | | | $B_g$ | 294 vw | 297 vw | 385 | $\omega(WO_2)$ |
| $B_u$ | | 283 vw | 280(281) | 282 vw | 263 | | | | | T′(Mn) |
| | | | | | | $B_g$ | 272 vw | 272 vw | 292 | $\rho(WO_2)$ + T′(Mn) |
| | | | | | | $A_g$ | 258 w | 261 w | 312 | $\tau(WO_2)$ |
| $B_u$ | 253 (277) | 254 s | 248 (273) | 253 s | 206 | | | | | T′(Mn) + T′(W) |
| $B_u$ | 209 (220) | 211 m | | 209 m | 186 | | | | | $\rho(WO_2)$ + T′(Mn) |
| | | | | | | $A_g$ | 206 w | 207 w | 206 | T′(Mn) |
| $A_u$ | 180 (194) | 188 m | 182 (192) | 185 m | 156 | | | | | T′(Mn) + T′(W) |
| | | | | | | $B_g$ | 178 vw | 178 vw | 217 | T′(Mn) |
| | | | | | | $B_g$ | 166 vw | 168 vw | 207 | T′(Mn) + T′(W) |
| | | | | | | $B_g$ | 160 vw | 158 vw | 189 | T′(Mn) + T′(W) |
| $B_u$ | 141 (153) | 146 m | 152 (157) | 146 m | 163 | | | | | $\omega(WO_2)$ |
| | | | | | | $A_g$ | 129 m | 130 m | 98 | T′(W) |
| | | | | | | $B_g$ | 90 vw | 91 vw | 113 | T′(W) |

The initial lattice parameters and atomic positions for the $MnWO_4$ structure were taken from the experimental data.[28] The initial values of the all parameters for the tungsten ions were assumed to be the same as those reported previously for $NaBi(WO_4)_2$.[31] Since the parameter *a* reflects the radii, it was obtained for the $Mn^{2+}$ ion by using the value for the $W^{6+}$ ion, i.e. $a_{Mn} = a_W r_{Mn}/r_W$, where *r* denotes the ionic radius. The initial parameters (except those of parameters *b* and *c*) were changed during the calculations in small steps in order to obtain the best agreement between the observed and calculated wave numbers. The final parameters used in the present calculations are listed in Table II.

Raman spectra of the studied crystals are in very good agreement with previously reported data. The weak band near 924 $cm^{-1}$, which was assigned previously to some impurity phase,[22] is also observed for our samples. The number of observed IR bands for the polycrystalline samples is in good agreement with predictions but also in this case one additional

TABLE II. Potential parameters used in the lattice dynamic calculations.

| *i*th ion | $z_i$ (e) | $a_i$ (Å) | $b_i$ (Å) | $C$ (kcal$^{1/2}$ Å$^3$ mol$^{-1/2}$) |
|---|---|---|---|---|
| W | 2.8 | 0.954 | 0.10 | 0 |
| Mn | 1.6 | 1.214 | 0.08 | 0 |
| O1 | −1.1 | 1.826 | 0.16 | 20 |
| O2 | −1.1 | 1.826 | 0.16 | 20 |
| Ion pair | $D_{ij}$ (kcal mol$^{-1}$ | $\beta_{ij}$ (Å) | $r^*_{ij}$ (Å) | |
| W—O | 28.5 | 2.15 | 1.99 | |

shoulder is observed near 905 $cm^{-1}$, which can most likely be attributed to an impurity phase. Our polarized spectra allowed us to establish unambiguously symmetries of all observed IR bands (see Table I). It is worth noting that the reflectivity data show two additional and weak bands at 885 and near 735 $cm^{-1}$, which are not observed in the polycrystalline spectra. The origin of these bands is not clear. Comparison of our results with recently reported reflectivity data for $MnWO_4$ show that Choi *et al.* correctly predicted which bands belong to the $A_u$ modes.[24] However, data for $B_u$ modes are not correct. For instance, according to Choi *et al.*, above 530 $cm^{-1}$, only two $B_u$ modes are located at 845–853 and 652–668 $cm^{-1}$, e.g., at wave numbers very similar to those of the $A_u$ modes (861 and 661 $cm^{-1}$).[24] Therefore, according to these results one could expect to observe only two bands in the polycrystalline spectrum above 530 $cm^{-1}$. However, our results show that there are four well-separated bands in this region for polycrystalline samples (see Fig. 3) and TO modes of $B_u$ symmetry are expected at 577 and 795 $cm^{-1}$. We established that the symmetry of the observed IR modes is further supported by LD calculations.

Results of our LD calculations and polarized studies allow us to propose a detailed assignment of modes to the respective motions of atoms (see Table I). The main conclusion from Table I is that the two highest wave number Raman and IR bands can be assigned to stretching modes of the short W–O2 bonds. Bands in the 390–710-$cm^{-1}$ region can be assigned to the stretching and bending modes of the double oxygen bridge and those at 290–380 $cm^{-1}$ to the bending modes of the $WO_2$ groups. Some of the bands below 290 $cm^{-1}$ also correspond to the bending modes of the $WO_2$ groups, but most of bands in the region have a strong contribution of translational motions of Mn and W atoms (see Table I).

It is also worth noting that the observed absorption maxima in the spectra of the powdered samples show a systematic upshift in comparison with the TO values obtained from single-crystal reflectivity data. Such a shift of an IR band toward higher wave numbers, i.e., toward the LO value, is often observed for powdered spectra of ionic crystals due to the depolarization field, which appears in small crystallites.[32]

### C. Magnetization and specific heat

Figure 4(a) presents the temperature dependence of the magnetization $M(T)$ of a $Mn_{0.85}Co_{0.15}WO_4$ crystal. The change of slope near 16.2 K is an evidence of a magnetic ordering that occurs in the compound. This phase transition can be better observed in the temperature derivative $dM/dT$ presented in the inset in Fig. 4(a). The value of $T_N$ is in good agreement with the 17 K value reported by Chaudhury *et al.*, and, according to the literature data, this second-order phase transition leads to a simple collinear antiferromagnetic phase AF4.[16] With a further lowering of temperature, clear anomalies are visible at about $T_c = 10.5$ K and $T_2 = 7.5$ K. According to Chaudhury *et al.* the major phase between $T_c$ and $T_2$ is the AF1 phase, but this phase does coexist with the AF2 phase.[16] In contrast to this statement, Song *et al.* reported that in this temperature range phases AF2′ and AF4 coexist.[14] Song *et al.* could not observe the phase transition at about 7 K but according to Chaudhury *et al.* the AF2 phase is still present below $T_2$, although the

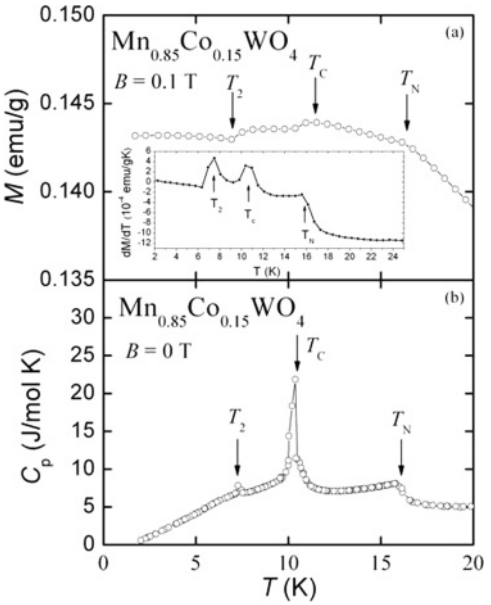


FIG. 4. Low-temperature magnetization $M$ (upper panel) and specific heat $C_p$ (lower panel) of a $Mn_{0.85}Co_{0.15}WO_4$ single crystal as a function of temperature $T$, measured in the external magnetic field $B$. The arrows mark the phase transition temperatures. The inset in panel (a) shows the temperature derivative of magnetization.

major phase is now the incommensurate AF5 phase.[14–16] The three phase transitions can also be well observed by specific heat measurements as distinct anomalies at 16.0, 10.2, and 7.3 K [see Fig. 4(b)]. Very similar values were reported by Chaudhury *et al.*[16] The shapes of the anomalies at 16.0 and 10.2 K are very similar to those observed previously, but the absolute value of the specific heat at 10.2 K is about 50% larger than that reported in literature.[16] On the other hand, the specific heat anomaly at 7.3 K is much weaker that reported previously.[16] Former studies of undoped $MnWO_4$ showed that the phase transitions at $T_{N3}$ and $T_{N2}$ are little affected by the quality of crystals.[4,6] However, some impurities present in the crystals grown from flux or polycrystalline samples weakened the anomaly at $T_{N1}$ and shifted the transition temperature toward lower temperatures.[4,6] It was concluded that impurities stabilized the ferroelectric AF2 phase.[4,6] Recent studies of $MnWO_4$ doped with $Zn^{2+}$ ions also showed similar behavior and a complete suppression of the low-temperature AF1 phase for $Mn_{0.95}Zn_{0.05}WO_4$.[33] We suppose, therefore, that the observed difference in the behavior of our flux-grown $Mn_{0.85}Co_{0.15}WO_4$ crystal and that studied by the floating-zone-grown $Mn_{0.85}Co_{0.15}WO_4$ crystal of Chaudhury *et al.* can be attributed to the presence of some impurities in our sample. However, it seems that the concentrations of some impurities are small since the phase transition at 7.3 K is still clearly observed.

### D. Temperature dependence of Raman- and IR-active modes of $Mn_{0.97}Fe_{0.3}WO_4$

Raman and IR spectra of $Mn_{0.97}Fe_{0.03}WO_4$ at a few temperatures are presented in Figs. 5(a) and 6, respectively. All temperature-dependent infrared spectra are unpolarized since they were measured for powdered samples. Figures 7–10

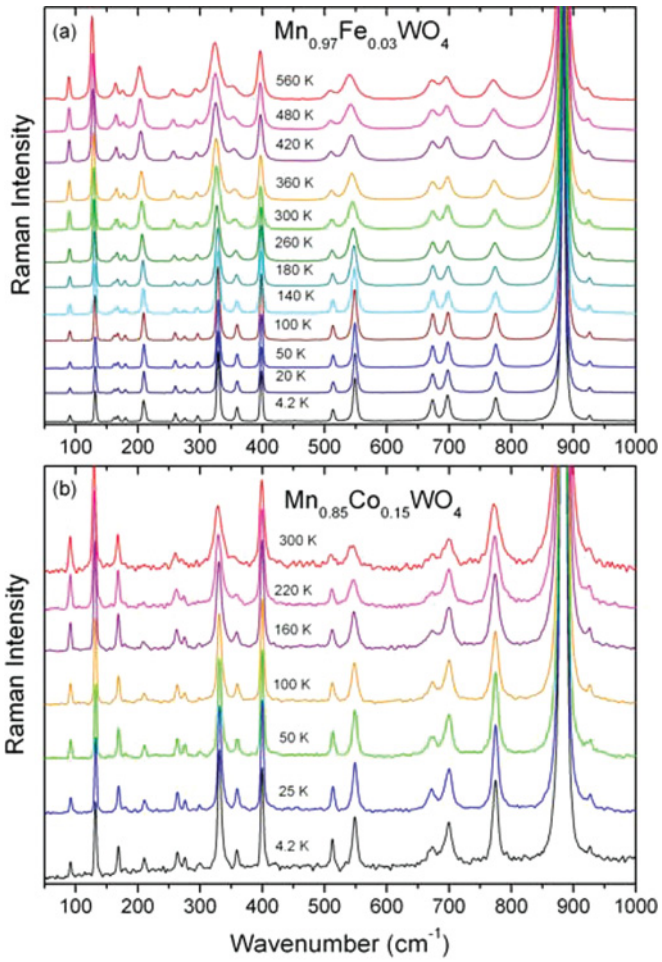


FIG. 5. (Color online) Raman spectra of $Mn_{0.97}Fe_{0.03}WO_4$ single crystals at a few temperatures in (a) a(bb+bc)a scattering geometry and (b) $Mn_{0.85}Co_{0.15}WO_4$ single crystals in c(aa+ba)c scattering geometry. Spectra at 4.2 K were recorded for the samples immersed in liquid helium.

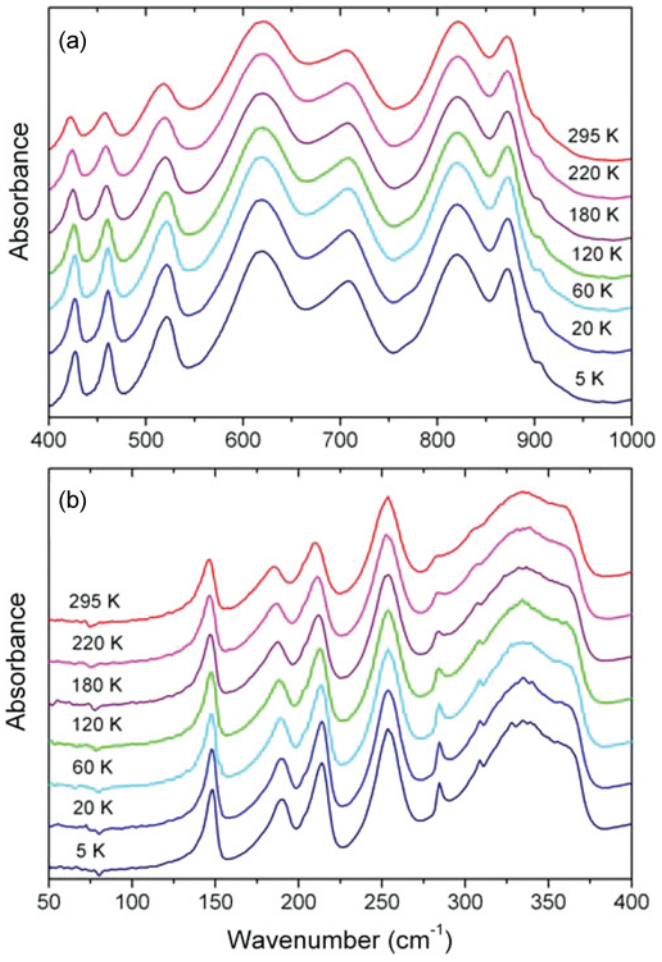


FIG. 6. (Color online) Unpolarized (a) mid-IR and (b) far-IR spectra of $Mn_{0.97}Fe_{0.03}WO_4$ at a few temperatures.

show the temperature dependence of Raman and IR linewidths (full-width at half-maximum, FWHM) and wave numbers. It can be seen that the bands broaden monotonously with increasing temperature but damping of the 872- and 706-$cm^{-1}$ IR modes show additional, weak anomalies below 50 K. The temperature evolution of many Raman and IR wave numbers is unconventional in several aspects. First, a continuous hardening is observed upon heating for the 821- and 620-$cm^{-1}$ IR modes (Fig. 10). Second, for the 884-, 698-, and 673-$cm^{-1}$ Raman modes an initial hardening is followed, above a certain crossover temperature, by the more common behavior of mode softening with increasing temperature (Fig. 9). Third, nearly all modes show additional weak anomalies below 20 K (Figs. 9 and 10). It is worth noting that Iliev *et al.* could not observe any anomalous behaviors of Raman bands for this flux-grown $MnWO_4$ crystals.[22] On the other hand, Hoang *et al.* observed similar broad anomalies for the 884-, 698-, and 673-$cm^{-1}$ Raman modes of the $MnWO_4$ crystals grown by the floating zone method but no weak anomalies below 20 K.[23]

Damping of phonons can be attributed to disorder, phonon-phonon, spin-phonon, or CF-phonon couplings.[17,20,34–38] The first and fourth contributions can be neglected because x-ray studies have shown that the $MnWO_4$ structure is well ordered and there are no CF levels below 1000 $cm^{-1}$.[24,28] Thus the change in damping with temperature is expected to come mainly from spin-phonon and phonon-phonon anharmonic contributions. Since, however, magnetic ordering in $MnWO_4$ occurs at very low temperatures, the spin-phonon coupling may contribute weakly to the observed damping of phonon modes only at low temperatures.

The contribution of the third-order anharmonicity to the linewidths, under the assumption that decay occurs to two phonons of frequency $\omega_1$ and $\omega_2$, amounts to[38]

$$\Gamma(T) = \Gamma_0 + A\left(1 + \frac{1}{e^{x_1} - 1} + \frac{1}{e^{x_2} - 1}\right), \qquad (6)$$

where $x_1 = hc\omega_1/k_BT, x_2 = hc\omega_2/k_BT$. $h$, $c$, $k_B$, and $T$ denote Planck's constant, the speed of light, Boltzmann's constant, and the temperature, respectively. $\Gamma_0$ accounts for the broadening arising from factors other than the phonon decay, such as structural or compositional defects. The coefficient $A$ is an adjustable parameter that represents the strengths of the third-order phonon-phonon interactions. Figures 7(a) and 8 show that the temperature dependences of both Raman and IR linewidths can be well approximated by Eq. (6), except in the low-temperature range, where the 872-, and 706-$cm^{-1}$ IR modes show additional, weak anomalies. This additional

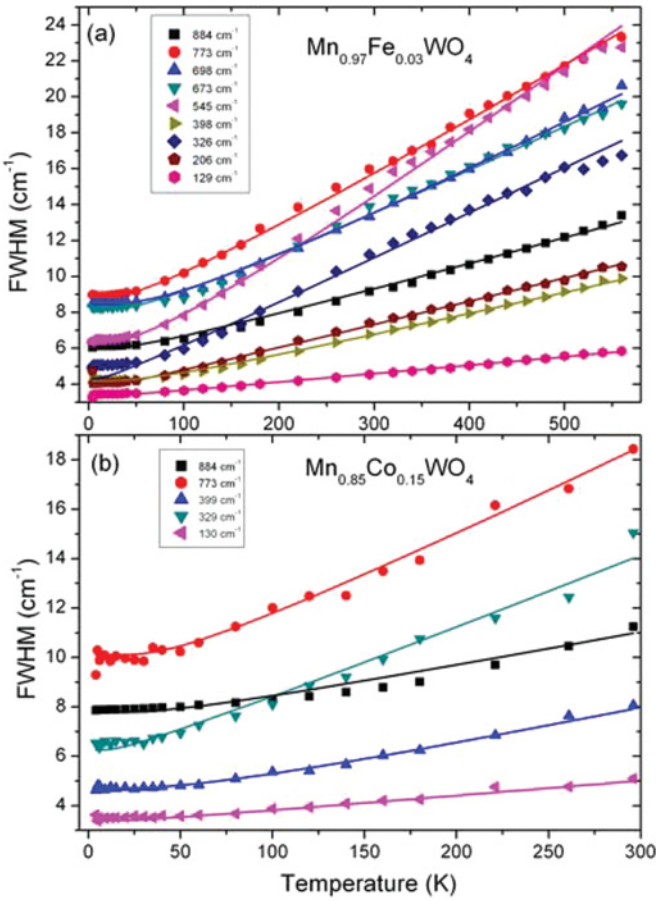


FIG. 7. (Color online) Temperature dependence of linewidths of the Raman bands of (a) $Mn_{0.97}Fe_{0.03}WO_4$ and (b) $Mn_{0.85}Co_{0.15}WO_4$. Solid lines correspond to the expected temperature dependence of the phonon linewidths due to phonon-phonon interactions.

contribution to the phonon-mode linewidths most likely comes from spin-phonon interactions.

The change in wave number of a phonon $i$ is also expected to come mainly from phonon-phonon anharmonic effects with an additional weaker contribution at low temperatures due to spin-phonon interactions and/or the onset of a long-range ferroelectric order. Taking into account only the phonon-phonon interactions, the wave number of a phonon $i$ is given by

$$\omega_i(T) = \omega_{i0} + (\Delta\omega_i)_{latt} + (\Delta\omega_i)_{anh} \quad (7)$$

where $\omega_{i0}$ is the harmonic frequency. The quasi-harmonic term $(\Delta\omega_i)_{\text{latt}}$ accounts for the change of the ionic binding energies due to lattice expansion and thermal evolution of other structural parameters, and $(\Delta\omega_i)_{\text{anh}}$ is the intrinsic (or *true*) anharmonic contribution.

The third term in Eq. (7), in the assumption of anharmonic decay of a phonon of frequencies $\omega$ to two phonons of frequencies $\omega_1$ and $\omega_2$ and three identical phonons of frequency $\omega/3$, is given by[38]

$$\Delta\omega_{i,\text{anh}}(T) = A\left(1 + \frac{1}{e^{x_1}-1} + \frac{1}{e^{x_2}-1}\right) + B\left(1 + \frac{3}{e^{x_3}-1} + \frac{3}{(e^{x_3}-1)^2}\right), \quad (8)$$

where $x_1$ and $x_2$ have the same meaning as in Eq. (6), $x_3 = hc\omega/3k_BT$, and $A$ and $B$ represent the strengths of third- and fourth-order decay, respectively. Depending on the magnitude and signs of $A$ and $B$ this contribution may be positive or negative. Figures 9 and 10 show that the temperature evolution of the majority of modes can be well explained assuming phonon-phonon anharmonic interaction, except of the lowest-temperature range. However, for the 884-, 698-, and 673-cm$^{-1}$ Raman modes, our attempts to model the observed downturn near 150–200 K resulted in a large error and an unreasonably large value of the $B$ coupling parameter. A similar problem occurs also for the 871-, and 620-cm$^{-1}$ IR modes. We conclude, therefore, that Eq. (8) alone cannot explain the temperature evolution of these modes below 150–200 K as well as low-temperature anomalies observed for some other modes.

As regards the lattice contribution (quasiharmonic term), it is usually expressed as

$$\Delta\omega^i_{qh}(T) = \omega^i_0\left\{\exp\left[-\int_0^T \gamma_i\alpha(T')dT'\right] - 1\right\}, \quad (9)$$

where

$$\gamma_i = -\frac{\partial \ln \omega_i}{\partial \ln V}$$

is the Grüneisen parameter of mode $i$ and

$$\alpha(T) = \frac{1}{V}\frac{\partial V}{\partial T}$$

is the coefficient of thermal expansion. If $\gamma$ and $\alpha$ are positive, the exponential is $<1$ and this contribution is negative.

Positive Grüneisen parameters $\gamma_i$ have been reported from Raman measurements under pressure and theoretical calculations for $ZnWO_4$, $CdWO_4$, and $MgWO_4$ wolframite-type crystals,[39–41] so that we may assume that they will also be positive for $MnWO_4$. In the case of IR modes, negative $\gamma_i$ values were reported only for the three $B_u$ modes of $MgWO_4$ observed at the lowest wave numbers.[39] As regards thermal expansion, almost-constant lattice parameters are found at low $T$ ($\leqslant$50 K) for nonmagnetic $ZnWO_4$ followed by a positive lattice expansion above that temperature.[42] It is worth adding that the thermal expansion is anisotropic, i.e., in the 4–300 K range the parameters $a$, $b$, and $c$ increase by about 0.20%, 0.17%, and 0.10%, respectively.[42] Positive lattice expansion is also reported for $CdWO_4$.[43] Details of lattice expansion of $MnWO_4$ in a broad temperature range are not known. However, theoretical calculations suggest that $MnWO_4$ also should have a positive thermal expansion with the linear thermal expansion coefficient $\alpha$ very similar to that of $ZnWO_4$.[44] It is therefore reasonable to assume that lattice parameters of $MnWO_4$ also should increase with increasing temperature but some additional anomalies may appear at low-temperatures due to magnetic and/or ferroelectric order. Indeed, recent low-temperature thermal expansion studies of $MnWO_4$ showed anomalies at $T_{N3}$ and $T_{N1}$.[45] They also showed that the $a$ and $c$ parameters of the paramagnetic phase of $MnWO_4$ exhibit a positive thermal expansion in the 12.5–19 K range.[45] Interestingly, the parameter $b$ exhibits negative dependence in this temperature range, but this temperature dependence is weak and as a result $\alpha$ is slightly positive. Therefore, Eq. (9)

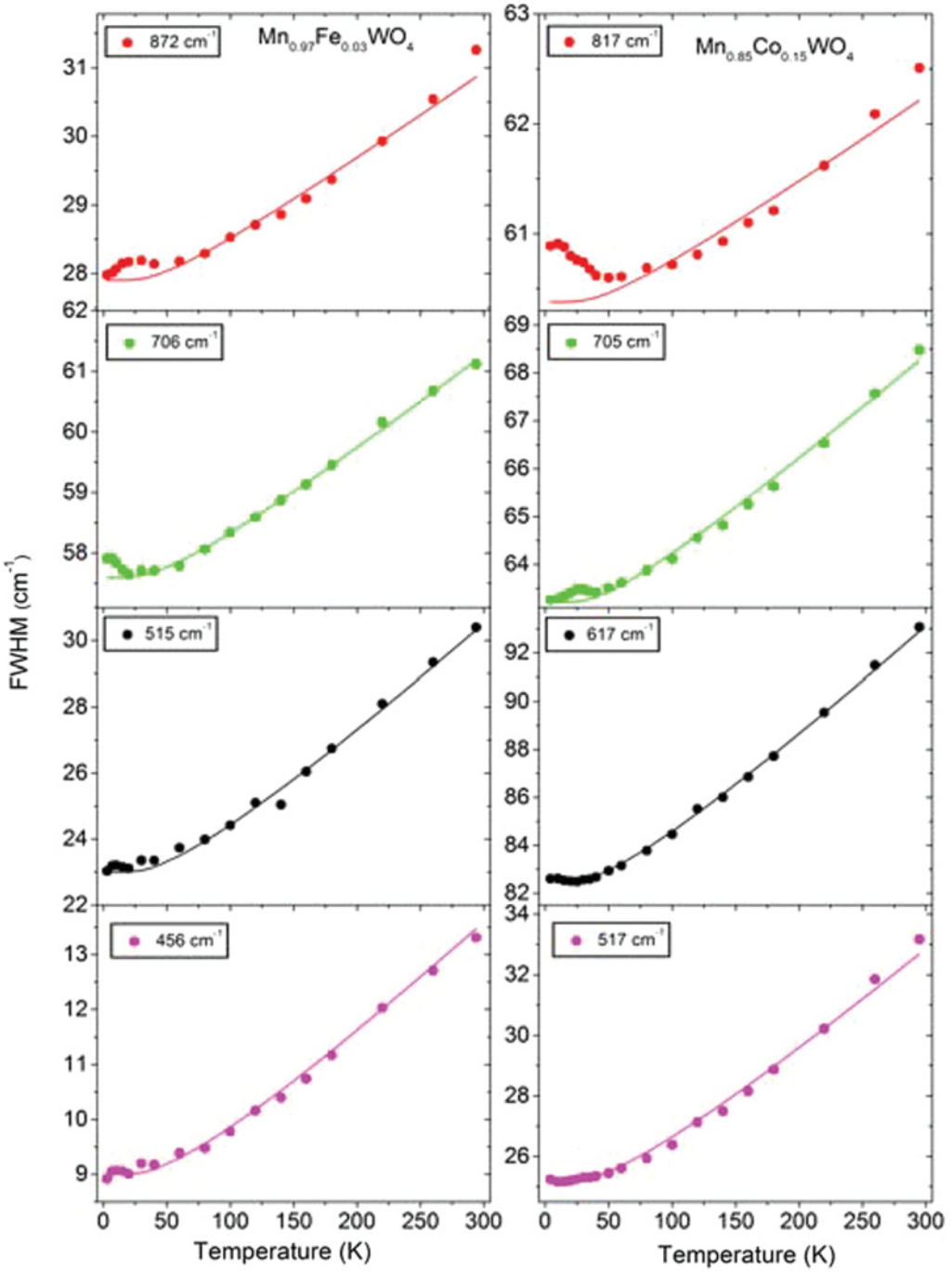


FIG. 8. (Color online) Temperature dependence of linewidths of some representative IR bands of $Mn_{0.97}Fe_{0.03}WO_4$ (left panels) and $Mn_{0.85}Co_{0.15}WO_4$ (right panels). Solid lines correspond to the expected temperature dependence of the phonon linewidths due to phonon-phonon interactions.

alone predicts for the paramagnetic phase a weak softening of nearly all modes at low temperature followed by the usual softening with increasing temperatures above 50 K. The only exceptions are the three lowest wave-number IR modes, which may have negative $\gamma_i$ values. This prediction is contrary to the observation for the 821-, and 620-cm$^{-1}$ IR modes at any *T,* and for the 884-, 698-, and 673-cm$^{-1}$ Raman modes below 200-100 K.

In summary, the observed hardening of the 821- and 620-cm$^{-1}$ IR modes might be explained by means of both Eqs. (8) and (9) as a result of unusually strong and positive intrinsic anharmonicity. A combination of Eqs. (8) and (9) might also explain the behavior of the 884-, 698-, and 673-cm$^{-1}$ Raman modes at high temperatures, but not the downturn observed below 150–200 K for these modes as well as weak anomalies observed below 20 K for many other Raman and IR modes.

Let us at first discuss the possible origin of the observed downturn below 150–200 K for 884-, 698-, and 673-cm$^{-1}$ Raman modes. It is well known that the magnetic order may

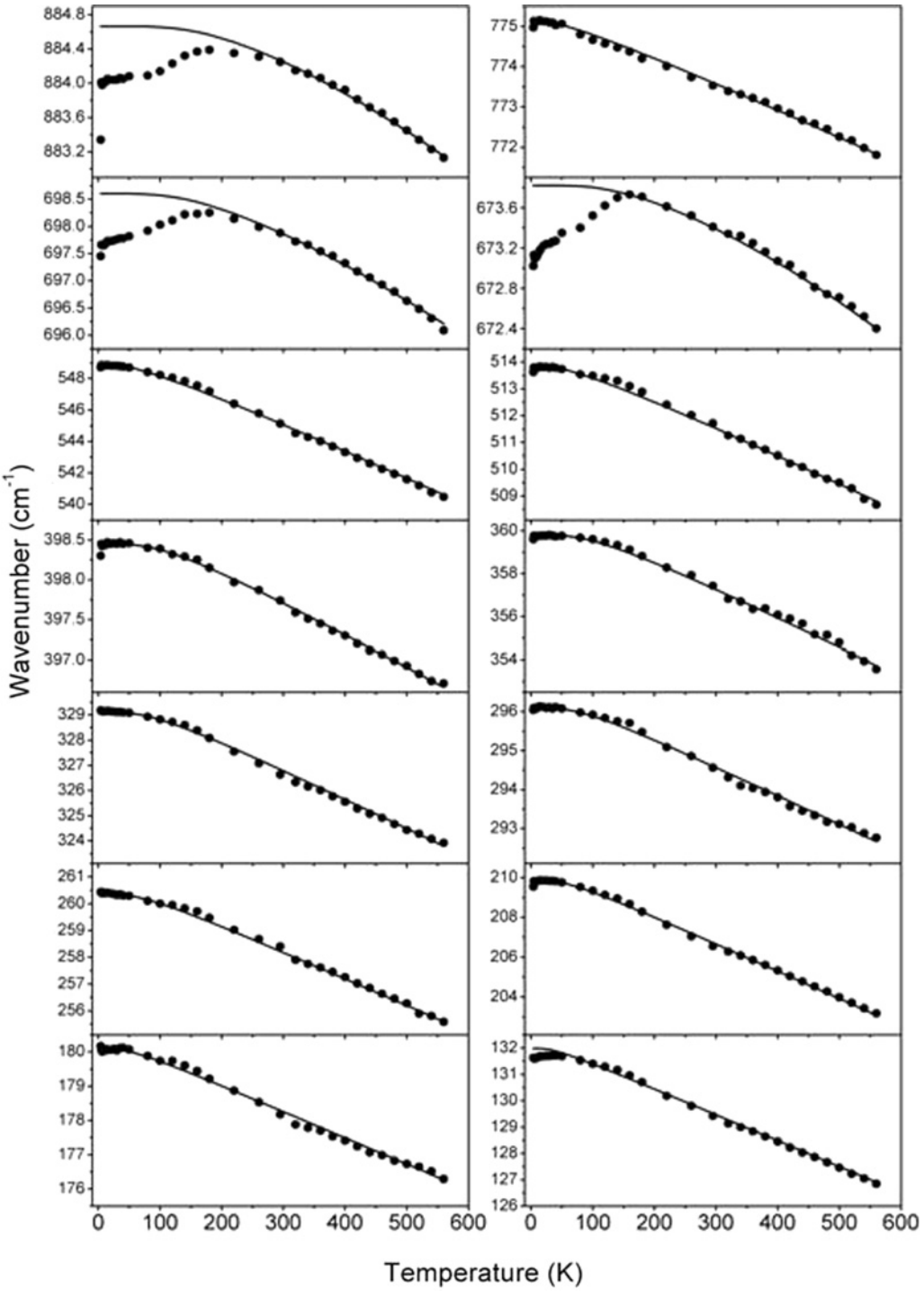


FIG. 9. Temperature dependence of Raman wave numbers of $Mn_{0.97}Fe_{0.03}WO_4$. Solid lines correspond to the expected temperature dependence of the phonon wave numbers due to phonon-phonon interactions.

couple to the phonon modes through a modulation of the exchange integral by the lattice vibrations. An additional shift of a Raman band due to this coupling, $\Delta\omega_{\text{s-ph}}$, was shown to be proportional to $\lambda\langle S_i S_j\rangle$, where $\langle S_i S_j\rangle$ is the spin correlation function and $\lambda$ is the spin-phonon coupling coefficient, and to the second derivative of the exchange integral with respect to the normal coordinate of the phonon.[17,20,35–37,46,47] In conventional magnetic systems both contributions are negligible above $T_N$, and therefore no anomalous phonon shifts are expected in the paramagnetic phase. However, in magnetically frustrated systems the second contribution may become important.[17,20] For instance, it was shown to be important for $RMnO_3$ and $RMn_2O_5$ manganites (R = rare earth, Bi), which show inherent magnetic frustration caused by the lattice geometry.[17,20] For these materials the anomalous phonon shifts were observed up to 50 K above $T_N$.[17,20] $MnWO_4$ is also

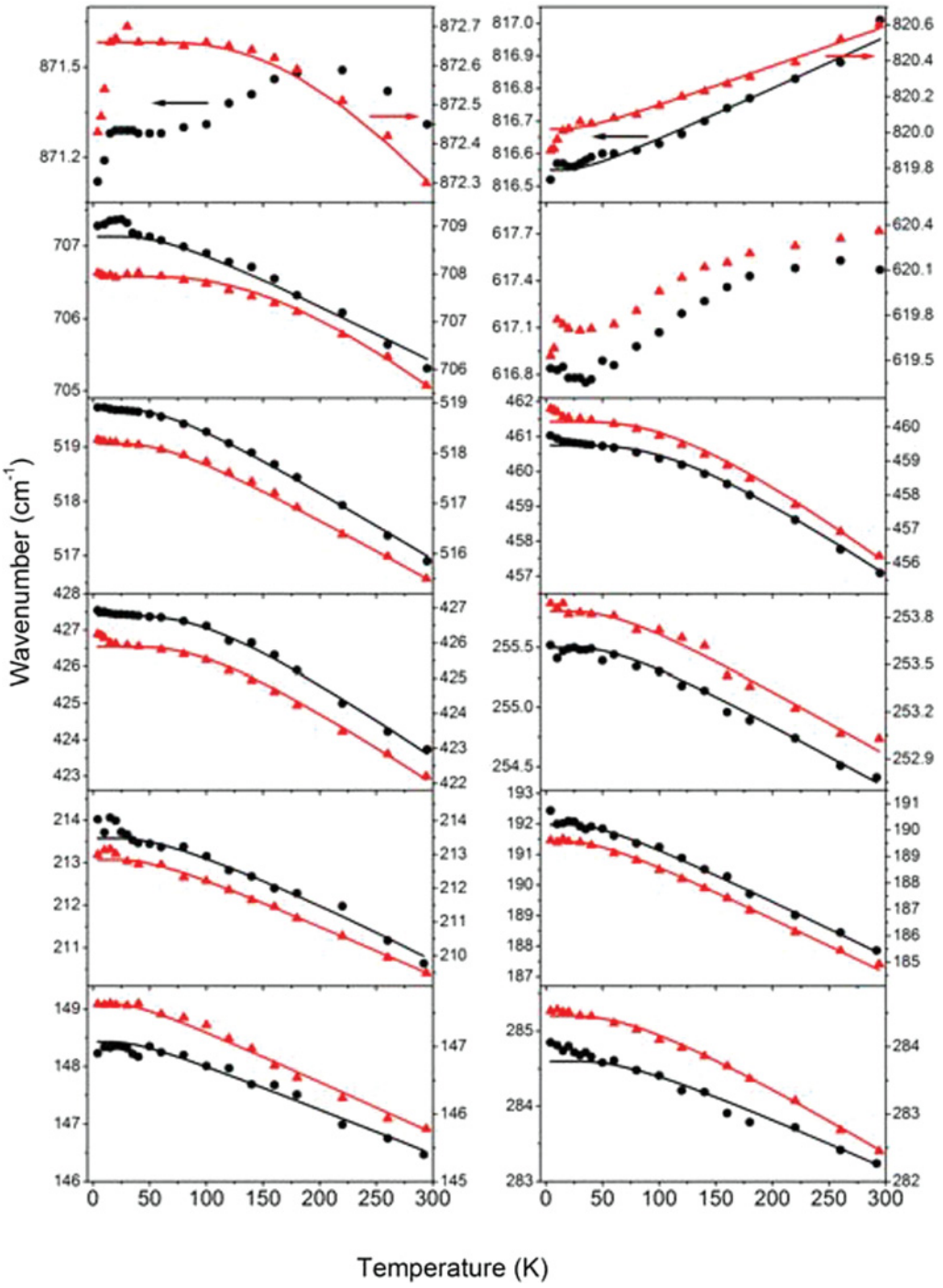


FIG. 10. (Color online) Temperature dependence of IR wave numbers of $Mn_{0.97}Fe_{0.03}WO_4$ (triangles) and $Mn_{0.85}Co_{0.15}WO_4$ (circles). Solid lines correspond to the expected temperature dependence of the phonon wave numbers due to phonon-phonon interactions.

known to be a moderately frustrated antiferromagnetic system with frustration parameter $\approx 5$.[6] Therefore, some anomalous phonon shifts are also expected for $Mn_{0.97}Fe_{0.03}WO_4$ above $T_{N3} \approx 12$ K. However, the anomalous softening of the 884-, 698-, and 673-cm$^{-1}$ Raman modes extends up to 150–200 K, i.e., it is observed at much higher temperatures than expected for magnetic correlations. We suppose, therefore, that there is also another, nonmagnetic contribution. Hoang *et al.,* who also observed a similar downturn for these Raman modes, related this anomaly with microscopic structural change because according to their results this anomaly is associated with the disappearance of the 179-cm$^{-1}$ mode at about 180 K.[23] Our results show very clearly that the mode at 179 cm$^{-1}$ does not disappear at 180 K and therefore we cannot confirm the presence of any structural phase transition in this material near 180 K. Here it is important to remember that Eq. (9) is applicable for cubic crystals whereas for the monoclinic $Mn_{0.97}Fe_{0.03}WO_4$ crystal studied here the thermal expansion

is expected to be highly anisotropic (see discussion above). Therefore, the observed anomaly may be most likely attributed, at least partially, to an anisotropic character of the thermal expansion and the corresponding subtle structural changes, i.e., changes in the bond angles and distortion of the structural polyhedra. Careful XRD studies at different temperatures may help to elucidate the origin of this anomaly.

As mentioned above, our results show additional weak phonon shifts below 20 K, as compared with normal anharmonic behavior. These shifts are negative for all Raman bands and are less than 0.7 $cm^{-1}$. In contrast to this behavior, IR bands show both positive and negative shifts less than 0.3 $cm^{-1}$. Temperature-dependent Raman studies of nonmagnetic $ZnWO_4$, which also crystallizes in the wolframite-type structure, did not reveal any low-temperature anomalies.[48] It is therefore plausible to assume that these additional phonon shifts appear due to spin-phonon coupling in the magnetically ordered phases. The second possibility is that the observed anomalies are consequences of the Mn displacements and/or lattice anomalies that occur at the ferroelectric transition temperature. It has been reported previously that the ferroelectric polarization and lattice anomalies at the phase transitions are small. For instance, when the temperature decreases from 16 to 7.5 K, lattice parameters change continuously and the relative changes are $\Delta a/a \approx -1.5 \times 10^{-4}$, $\Delta b/b \approx 2 \times 10^{-5}$, and $\Delta c/c \approx -5 \times 10^{-5}$.[45] Since a slightly positive thermal expansion is observed for only the $b$ parameter, the unit cell volume decreases. At $T_{N1}$ the changes are discontinuous but small: $\Delta a/a \approx -3 \times 10^{-5}$, $\Delta b/b \approx -1 \times 10^{-5}$, $\Delta c/c \approx 1 \times 10^{-5}$ and $\Delta V/V \approx -3 \times 10^{-5}$.[45] As one can notice, the volume decreases with decreasing temperature below $T_{N3}$, and therefore lattice anomalies related to the phase transitions do not explain the observed anomalous softening of Raman and IR modes. Since the spin-phonon coupling $\lambda$ is different for different phonons, and it may be both positive and negative, the spin-phonon coupling may lead to softening of some phonons and hardening of other phonons. We attribute, therefore, the observed anomalies below 20 K mainly to spin-phonon coupling. Another argument for these anomalies being attributed to spin-phonon coupling rather than to the onset of ferroelectric order is that the anomalous behavior becomes evident well above the temperature of ferroelectric ordering.

### E. Temperature dependence of Raman- and IR-active modes of $Mn_{0.85}Co_{0.15}WO_4$

Raman and IR spectra of $Mn_{0.85}Co_{0.15}WO_4$ at a few temperatures are presented in Figs. 5(b) and 11, respectively. Figures 7(b), 8, 10, and 12 show the temperature dependence, of Raman and IR linewidths and wave numbers. The comparison of the obtained data for $Mn_{0.85}Co_{0.15}WO_4$ with those obtained for $Mn_{0.97}Fe_{0.03}WO_4$ shows that temperature dependences of the majority of modes are similar for these crystals (see Figs. 7–10 and 12). However, there are also some differences. First, the linewidths of $Mn_{0.85}Co_{0.15}WO_4$ are significantly larger compared with $Mn_{0.97}Fe_{0.03}WO_4$ due to substitutional disorder induced by a larger concentration of dopant ions in the $MnWO_4$ lattice. Second, the linewidth of the 705 $cm^{-1}$ IR band of $Mn_{0.85}Co_{0.15}WO_4$ exhibits a weak anomalous maximum at about 25 K whereas it shows a

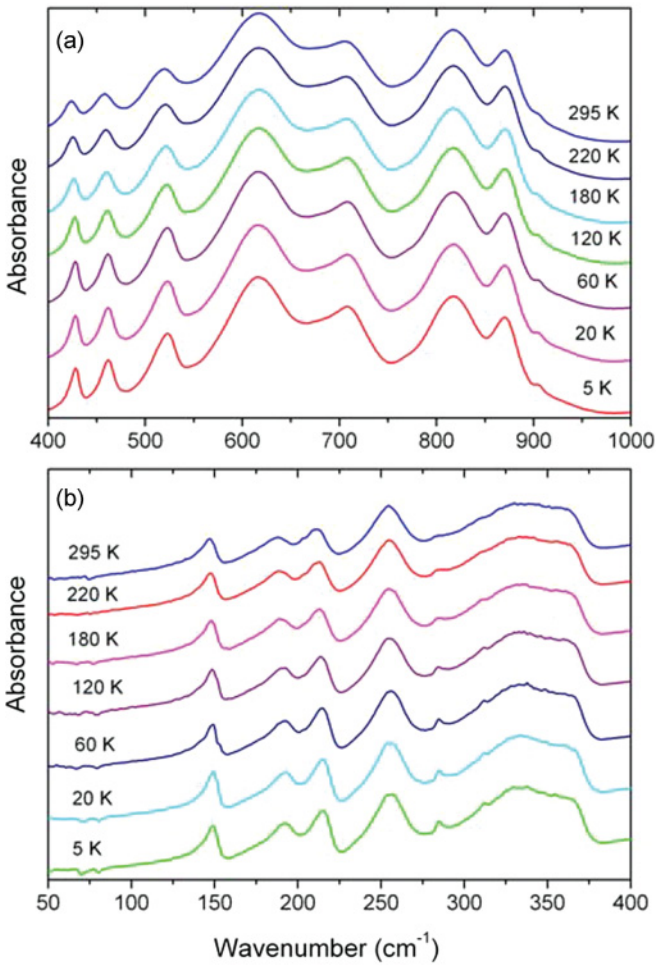


FIG. 11. (Color online) Unpolarized (a) mid-IR and (b) far-IR spectra of $Mn_{0.85}Co_{0.15}WO_4$ at a few temperatures.

weak increase below 20 K for $Mn_{0.97}Fe_{0.03}WO_4$. Third, for the 871-$cm^{-1}$ IR band an initial hardening above 50 K is followed by softening above 180–250 K with increasing temperature. The corresponding 872-$cm^{-1}$ band of $Mn_{0.97}Fe_{0.03}WO_4$ shows softening above 40 K without any crossover at higher temperature. Fourth, the downshift (upshift) exhibited by the 817- (457- and 424-) $cm^{-1}$ IR bands below 20 K is more pronounced for the $Mn_{0.97}Fe_{0.03}WO_4$ when compared with $Mn_{0.85}Co_{0.15}WO_4$. Similar behavior is observed for the 884-$cm^{-1}$ Raman band. Fifth, the 620-$cm^{-1}$ IR band of $Mn_{0.85}Co_{0.15}WO_4$ exhibits a weak upshift below 40 K whereas the corresponding band of $Mn_{0.97}Fe_{0.03}WO_4$ exhibits a weak upshift in the 30–10 K range followed by a downshift below 10 K. Sixth, the 705-$cm^{-1}$ IR band of $Mn_{0.85}Co_{0.15}WO_4$ exhibits a weak upshift below 35 K followed by a downshift below 35 K. The corresponding band of $Mn_{0.97}Fe_{0.03}WO_4$ exhibits a weak downshift in the 40–20 K range followed by an upshift below 20 K.

Raman and IR results show that many bands of $Mn_{0.85}Co_{0.15}WO_4$, especially in the low-wave-number region, shift with larger wave numbers compared with $Mn_{0.97}Fe_{0.03}WO_4$. This shift is consistent with the reported previously decrease of the unit-cell volume of $MnWO_4$ with $Co^{2+}$ doping. Our data also show that some modes

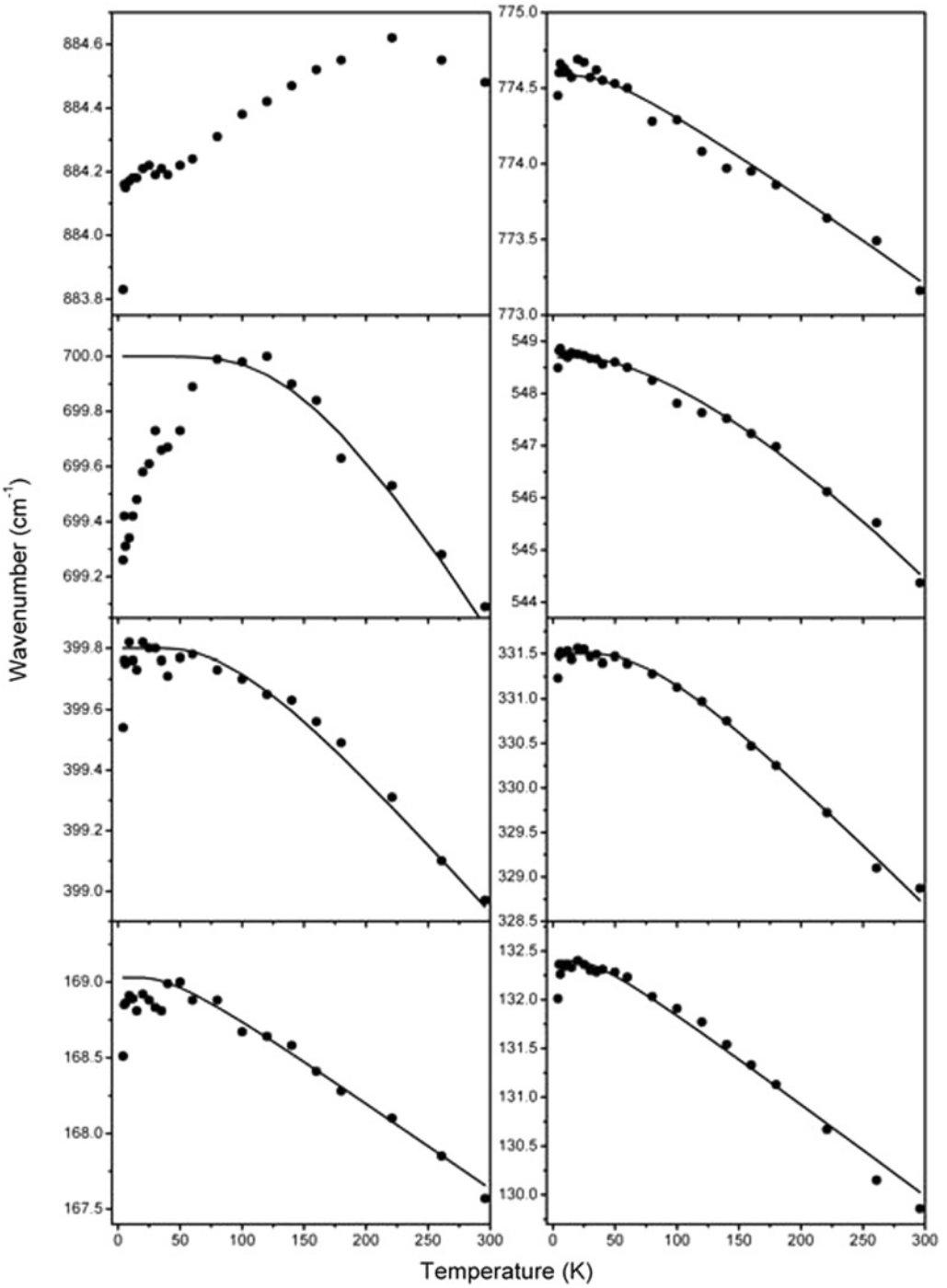


FIG. 12. Temperature dependence of Raman wave numbers of $Mn_{0.85}Co_{0.15}WO_4$. Solid lines correspond to the expected temperature dependence of the phonon wave numbers due to phonon-phonon interactions.

of $Mn_{0.85}Co_{0.15}WO_4$ exhibit a characteristic crossover from anomalous hardening to normal softening with increasing temperature near 180–250 K. Such behavior is also observed for $Mn_{0.97}Fe_{0.03}WO_4$ but the crossover occurs at different temperatures and it is observed for more phonons in the case of $Mn_{0.85}Co_{0.15}WO_4$. As mentioned above, the observed anomaly may be most likely attributed mainly to an anisotropic character of the thermal expansion and the corresponding changes in the bond angles and distortion of the structural polyhedra. The different behavior of $Mn_{0.85}Co_{0.15}WO_4$ and $Mn_{0.97}Fe_{0.03}WO_4$ is consistent with this conclusion since it was reported previously that the temperature coefficients of the lattice parameters and distortion of the $MnO_6$ octahedra change significantly with $Co^{2+}$ doping.[14] Our results also show significant differences in the anomalies observed below 50 K for both crystals. These differences reflect differences in the magnetic properties and phase transitions in these crystals, which affect the spin-phonon interactions. Interestingly,

the observed anomalies in the temperature dependence of some phonon shifts are weaker for $Mn_{0.85}Co_{0.15}WO_4$ compared with $Mn_{0.97}Fe_{0.03}WO_4$. This may be due to the more rigid zigzag chains of edge-shared $MnO_6$ octahedra in $Mn_{0.85}Co_{0.15}WO_4$, which leads to maintaining the balance among various exchange interactions, as suggested recently by Song *et al.*[15]

## IV. CONCLUSIONS

Room-temperature polarized Raman and IR studies of $Mn_{0.97}Fe_{0.03}WO_4$ and $Mn_{0.85}Co_{0.15}WO_4$ single crystals were performed. Symmetries of all IR-active modes were established, and the assignment of the modes to respective motions of atoms was proposed on the basis of lattice-dynamics calculations. Temperature-dependent IR and Raman studies were also performed on these crystals down to liquid helium temperature with a focus on phonon anomalous behavior due to the onset of long-range magnetic and ferroelectric orders. Raman and IR studies were complemented by magnetization and specific heat measurements for $Mn_{0.85}Co_{0.15}WO_4$. Magnetization and specific heat measurements showed the presence of a first-order phase transition at 7.3 K, in agreement with former studies of Chaudhury *et al.*[16] but in contradiction to the studies of Song *et al.*[14,15] Raman and IR results did not give any indication for the appearance of additional band or band splitting at low temperatures, which could indicate the onset of ferroelectric order. This result can be attributed to the fact that the spontaneous polarization induced in $MnWO_4$ by spiral magnetic order is weak, and therefore the corresponding displacements of the Mn atoms and lattice anomalies that occur at the ferroelectric transition are also weak. However, both $Mn_{0.97}Fe_{0.03}WO_4$ and $Mn_{0.85}Co_{0.15}WO_4$ showed anomalous phonon shifts and weak anomalies in phonon damping below 50 K, which we attributed mainly to spin-phonon coupling. Our results also revealed an unusual downturn of phonon shifts below 100–200 K for some phonons. These additional anomalies are likely related to some subtle structural changes due to the anisotropic character of thermal expansion. However, it is also likely that the presence of some magnetic correlations in the paramagnetic phase also contributes partially to these anomalies through the spin-phonon coupling mechanism. We also showed that there are differences in the temperature dependences of Raman and IR-active phonons for $Mn_{0.97}Fe_{0.03}WO_4$ and $Mn_{0.85}Co_{0.15}WO_4$. These differences reflect differences in the magnetic and ferroelectric properties of the both crystals at low temperatures.


[1] G. Lawes, A. B. Harris, T. Kimura, N. Rogado, R. J. Cava, A. Aharony, O. Entin-Wohlman, T. Yildrim, M. Kenzelmann, C. Broholm, and A. P. Ramirez, Phys. Rev. Lett. **95**, 087205 (2005).

[2] T. Kimura, J. C. Lashley, and A. P. Ramirez, Phys. Rev. B **73**, 220401 (2006).

[3] T. Kimura, G. Lawes, T. Goto, Y. Tokura, and A. P. Ramirez, Phys. Rev. B **71**, 224425 (2005).

[4] O. Heyer, N. Hollmann, I. Klassen, S. Jodlauk, L. Bohaty, P. Becker, J. A. Mydosh, T. Lorenz, and D. Khomskii, J. Phys. Condens. Matter **18**, L471 (2006).

[5] K. Taniguchi, N. Abe, H. Sagayama, S. Otani, T. Takenobu, Y. Iwasa, and T. Arima, Phys. Rev. B **77**, 064408 (2008).

[6] A. H. Arkenbout, T. T. M. Palstra, T. Siegrist, and T. Kimura, Phys. Rev. B **74**, 184431 (2006).

[7] L. Zhang, C. Lu, Y. Wang, and Y. Cheng, Mater. Chem. Phys. **103**, 433 (2007).

[8] J. Maier, Solid State Ionics **175**, 7 (2004).

[9] H. Y. He, J. F. Huang, L. Y. Cao, and J. P. Wu, Desalination **252**, 66 (2010).

[10] Y. X. Zhou, H. B. Yao, Q. Zhang, J. Y. Gong, S. J. Liu, and S. H. Yu, Inorg. Chem. **48**, 1082 (2009).

[11] V. M. Gredescul, S. A. Gredescul, V. V. Eremenko, and V. M. Naumenko, J. Phys. Chem. Sol. **33**, 859 (1972).

[12] A. Kuzmin, J. Purans, and R. Kalendarev, Ferroelectrics **258**, 21 (2001).

[13] R. P. Chaudhury, B. Lorenz, Y. Q. Wang, Y. Y. Sun, and C. W. Chu, New J. Phys. **11**, 033036 (2009).

[14] Y. S. Song, J. H. Chung, J. M. S. Park, and Y. N. Choi, Phys. Rev. B **79**, 224415 (2009).

[15] Y. S. Song, L. Q. Yan, B. Lee, S. H. Chun, K. H. Kim, S. B. Kim, A. Nogami, T. Katsufuji, J. Schefer, and J.-H. Chung, Phys. Rev. B. **82**, 214418 (2010).

[16] R. P. Chaudhury, F. Ye, J. A. Fernandez-Baca, Y.-Q. Wang, Y. Y. Sun, B. Lorenz, H. A. Mook, and C. W. Chu, Phys. Rev. B **82**, 184422 (2010).

[17] J. Laverdiere, S. Jandl, A. A. Mukhin, V. Yu. Ivanov, V. G. Ivanov, and M. N. Iliev, Phys. Rev. B **73**, 214301 (2006).

[18] M. Mkaczka, M. L. Sanjuán, A. F. Fuentes, L. Macalik, J. Hanuza, K. Matsuhira, and Z. Hiroi, Phys. Rev. B **79**, 214437 (2009).

[19] P. S. Dobal and R. S. Katiyar, J. Raman Spectrosc. **33**, 405 (2002).

[20] A. F. Garcia-Flores, E. Granado, H. Martinho, R. R. Urbano, C. Rettori, E. I. Golovenchits, V. A. Sanina, S. B. Oseroff, S. Park, and S. W. Cheong, Phys. Rev. B **73**, 104411 (2006).

[21] S. Kamba, D. Nuzhnyy, M. Savinov, J. Sebek, J. Petzelt, J. Prokleska, R. Haumont, and J. Kreisel, Phys. Rev. B **75**, 024403 (2007).

[22] M. N. Iliev, M. M. Gospodinov, and A. P. Litvinchuk, Phys. Rev. B **80**, 212302 (2009).

[23] L. H. Hoang, N. T. M. Hien, W. S. Choi, Y. S. Lee, K. Taniguchi, T. Arima, S. Yoon, X. B. Chen, and I.-S. Yang, J. Raman Spectrosc. **41**, 1005 (2010).

[24] W. S. Choi, K. Taniguchi, S. J. Moon, S. S. A. Seo, T. Arima, H. Hoang, I. S. Yang, T. W. Noh, and Y. S. Lee, Phys. Rev. B **81**, 205111 (2010).

[25] P. Becker, L. Bohaty, H.J. Eichler, H. Rhee, and A.A. Kaminskii, Laser Phys. Lett. **4**, 884 (2007).

[26] B.M. Wanklyn, J. Mater. Sci. **7**, 813 (1972).

[27] A. Majchrowski, M. T. Borowiec, and E. Michalski, J. Cryst. Growth **264**, 201 (2004).

[28] J. Macavei and H. Schulz, Z. Kristallogr. **207**, 193 (1993).

[29] F. Gervais and P. Echegut, in *Incommensurate phases in dielectrics*, edited by R. Blinc and A. P. Levanyuk (North Holland, Amsterdam, 1986), p. 337.

[30]R. Nozaki, J. N. Kondo, C. Hirose, K. Domen, A. Wada, and Y. Morioka, J. Phys. Chem. B **105**, 3319 (2001).
[31]M. Maczka, E. P. Kokanyan, and J. Hanuza, J. Raman Spectrosc. **36**, 33 (2005).
[32]J. T. Luxon, D. J. Montgomery, and R. Summitt, Phys. Rev. **188**, 1345 (1969).
[33]R. P. Chaudhury, F. Ye, J. A. Fernandez-Baca, B. Lorenz, Y.-Q. Wang, Y. Y. Sun, H. A. Mook, and C. W. Chu, Phys. Rev. B **83**, 014401 (2010).
[34]N. J. Hess, B. D. Begg, S. D. Conradson, D. E. McCready, P. L. Gassman, and W. J. Weber, J. Phys. Chem B **106**, 4663 (2002).
[35]J. S. Bae, I.-S. Yang, J. S. Lee, T. W. Noh, T. Takeda, and R. Kano, Vib. Spectrosc. **42**, 284 (2006).
[36]J. M. Weselinova and A. T. Apostolov, J. Phys. Condens. Matt. **8**, 473 (1996).
[37]M. Maczka, M. L. Sanjuán, A. F. Fuentes, K. Hermanowicz, and J. Hanuza, Phys. Rev. B **78**, 134420 (2008).
[38]M. Balkanski, R. F. Wallis, and E. Haro, Phys. Rev. B **28**, 1928 (1983).
[39]J. Ruiz-Fuertes, S. López-Moreno, D. Errandonea, J. Pellicer-Porres, R. Lacomba-Perales, A. Segura, P. Rodríguez-Hernández, A. Muñoz, A. H. Romero, and J. Gonzáles, J. Appl. Phys. **107**, 083506 (2010).
[40]D. Errandonea, F. J. Manjón, N. Garro, P. Rodríguez-Hernández, S. Radescu, A. Mujica, A. Muñoz, and C. Y. Tu, Phys. Rev. B **78**, 054116 (2008).
[41]A. Jayaraman, S. Y. Wang, and S. K. Sharma, Curr. Sci. **69**, 44 (1995).
[42]D. M. Trots, A. Senyshyn, L. Vasylechko, R. Niewa, T. Vad, V. B. Mikhailik, and H. Kraous, J. Phys. Condens. Matter **21**, 325402 (2009).
[43]S. C. Sabharwal and J. Sangeeta, Cryst. Growth **216**, 535 (2000).
[44]H. Li and S. Zhou, S. Zhang, J. Solid State Chem. **180**, 589 (2007).
[45]R. P. Chaudhury, F. Yen, C. R. dela Cruz, B. Lorenz, Y. Q. Wang, Y. Y. Sun, and C. W. Chu, Phys. B **403**, 1428 (2008).
[46]J. S. Lee, T. W. Noh, J. S. Bae, In-Sang Yang, T. Takeda, and R. Kanno, Phys. Rev. B **69**, 214428 (2004).
[47]E. Granado, A. Garcia, J. A. Sanjurjo, C. Rettori, I. Torriani, F. Prado, R. D. Sanchez, A. Caneiro, and S. B. Oseroff, Phys. Rev. B **60**, 11879 (1999).
[48]H. Wang, F. D. Medina, Y. D. Zhou, and Q.N. Zhang, Phys. Rev. B **45**, 10356 (1992).